Article

Influence of the Surface Roughness of a Silicon Disk Resonator on Its Q-Factor

A. V. Yakuhina *, A. S. Kadochkin, D. V. Gorelov, V. V. Svetukhin, S. S. Generalov and V. V. Amelichev

Technological Centre, Scientific-Manufacturing Complex, Federal State Budgetary Scientific Institution, off. 7237 House. 1 bld. 7, Shokina Square, Zelenograd, 124489 Moscow, Russia; askadochkin@sv.ulsu.ru (A.S.K.); d.gorelov@tcen.ru (D.V.G.); V.Svetukhin@tcen.ru (V.V.S.); S.Generalov@tcen.ru (S.S.G.); V.Amelichev@tcen.ru (V.V.A.)

* Correspondence: A.Yakuhina@tcen.ru

Abstract: This article presents a silicon disk resonator of the whispering-gallery-mode (WGM) type. The calculated Q-factor of the silicon WGM resonator was 10^7. Two methods of studying the surface roughness of a silicon WGM resonator with a nonlinear profile by means of Helios 650 scanning electron microscope and Bruker atomic force microscope (AFM) are presented. The results obtained by the two methods agreed well with each other. A comparison of the surface roughness values of WGM resonators manufactured using different technological approaches is presented. Based on the obtained data, a preliminary estimated Q-factor calculation of the resonators was performed, which was refined by numerical calculation using the finite-difference time-domain (FDTD) method. The effect of the surface roughness of the resonator on its Q-factor was found. Reducing the surface roughness of the resonator from 30 nm to 1–2 nm led to an increase in its Q-factor from 10^4 to 10^7.

1. Introduction

Currently, research in the field of developing devices that use photons as the main carrier of information is gaining more and more relevance. A special place has been occupied by research related to the use of optical waveguides and resonators using whispering-gallery-mode (WGM) designs. The reason is that such waveguide structures have a high Q-factor and relatively low optical losses in combination with a small volume of the mode [1].

It is possible to build optical filters using WGM resonators [2], narrow-band lasers with external resonant feedback [3,4], tunable delay lines [5,6] used for buffering signals, optical or radio frequency (RF) phase arrays [7], sensors [8,9], the creation of micro-opto-electromechanical gyroscopic systems [10] and other applications in the field of integrated photonics [11]. The possibility of generating coherent frequency combs and forming solitons in optical microresonators [12,13] has the potential to create compact spectrometers [14,15], low-noise RF sources [16], as well as optical frequency synthesizers [17].

For all these applications, the high Q-factors of resonators in devices are crucial. The use of high-Q resonators allows reducing the threshold for generating a parametric comb, increasing time delays and the sensitivity of a refractive index during sensing and improving frequency discrimination.

The research and wide application of WGM waveguides and resonators directly depends on how accessible and reproducible their manufacturing technology will be. Typical ultra-high-quality (UHQ) resonators made in the form of microspheres and microtoroids, due to their design and technological features, cannot be integrated into photonic integrated circuits (PICs) [10]. In this regard, alternatives that are compatible with silicon technology were proposed.

Silicon is one of the most promising materials for generating Kerr frequency combs [13] in the near- and mid-infrared frequency range due to the high Kerr nonlinearity. However, the use of silicon microresonators is limited due to relatively low Q-factors in some spectral ranges [18].

In this article, we present a silicon disk resonator manufactured by silicon technology using group-processing methods, the calculated Q-factor of which is 10^7. In addition, we give a detailed description of the technique for studying the surface roughness of a silicon resonator with a nonlinear profile.

2. Fabrication

One of the main criteria in the development of a method for creating an ultrahigh-Q silicon disk resonator is the need for its implementation using silicon technologies and group-processing methods. The choice of design parameters, such as the value of the "undercut", ''legs'' and the angle of the wedge-shaped profile, was based on previous studies [19,20]. Figure 1 shows the schematic of the profile of the developed structure.
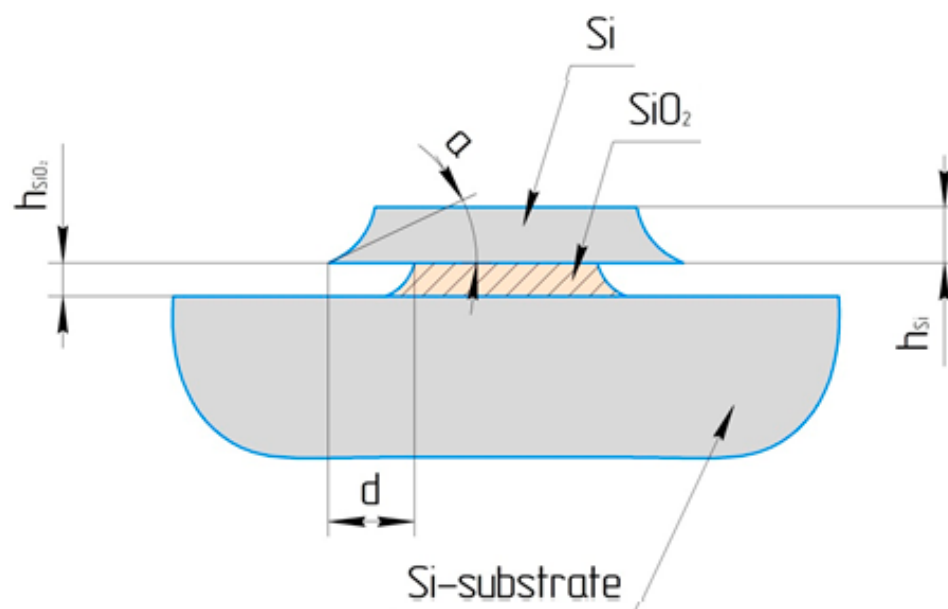

Figure 1. Schematic of the cross-section of the structure of a silicon whispering-gallery-mode (WGM) waveguide. Environment is air. h_{Si}, the thickness (height) of the wedge-shaped waveguide; h_{SiO2}, thickness (height) of the dielectric layer; d, distance from the edge of the wedge to the beginning of the oxide beam (support); a, wedge angle.

The topology of the resonators is formed by standard photolithography methods, followed by a set of standard technological processes used for the formation of integrated circuits and MEMS.

Figure 2 shows the SEM images of silicon disk WGM resonators with a wedge-shaped profile. In the SEM images presented, the surface of the resulting structure had minimal roughness. The estimation of the numerical value of the roughness is described in Section 3 of this article.
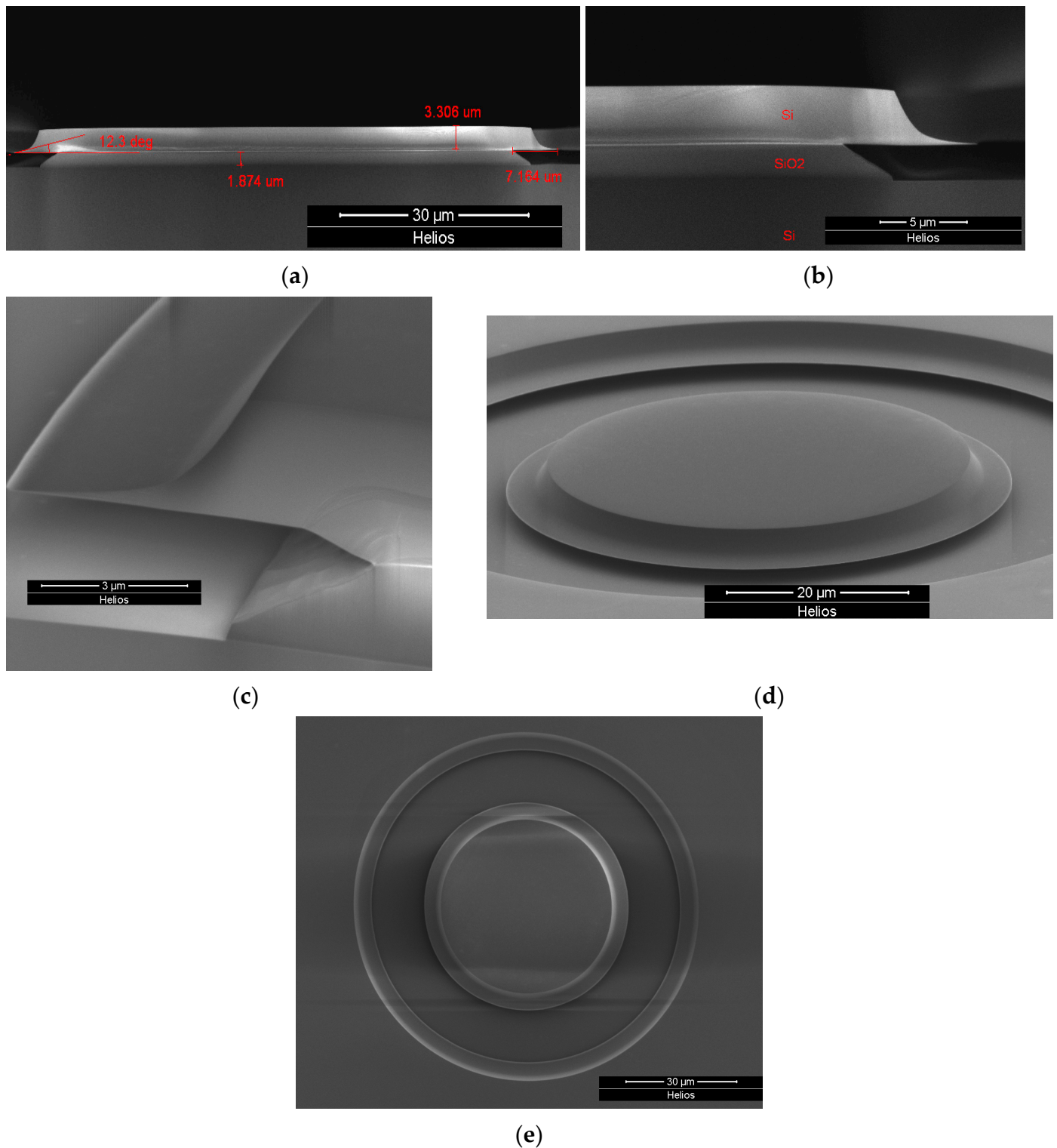
Figure 2. SEM images of silicon disk WGM resonators with a wedge-shaped profile: (**a**) cross-section of the structure of the silicon WGM resonator; (**b**) enlarged image of the wedge-shaped profile; (**c**) enlarged image of the surface of the formed silicon structure; (**d**) appearance; (**e**) top view.

The structures surrounding the WGM resonator were buffer technology areas. The value of the wedge-shaped profile angle was 12.3°, which is of particular interest for further studies of such a resonator. Using previously proven technology approaches, it was difficult

to achieve such a profile in silicon. These experimental results demonstrated the possibility of adjusting the angle and obtaining the lower surface roughness of the silicon resonator.

3. Evaluation of the Surface Roughness of Silicon Resonators

In order to establish the influence of the surface roughness of the resonator on the value of its Q-factor, a quantitative assessment of the surface roughness of the manufactured samples was performed using a Helios 650 scanning electron microscope. The research of Japanese authors [21,22], as well as previously presented developments [23], was taken as the basis for the development of the technique. The purpose of the method is to study the horizontal edge of an etched element.

3.1. Roughness Analysis Using a Helios 650 Scanning Electron Microscope

Cr and Pt layers were formed on the selected area of the studied structure, and then the area of study was removed using an ion beam (Figure 3).
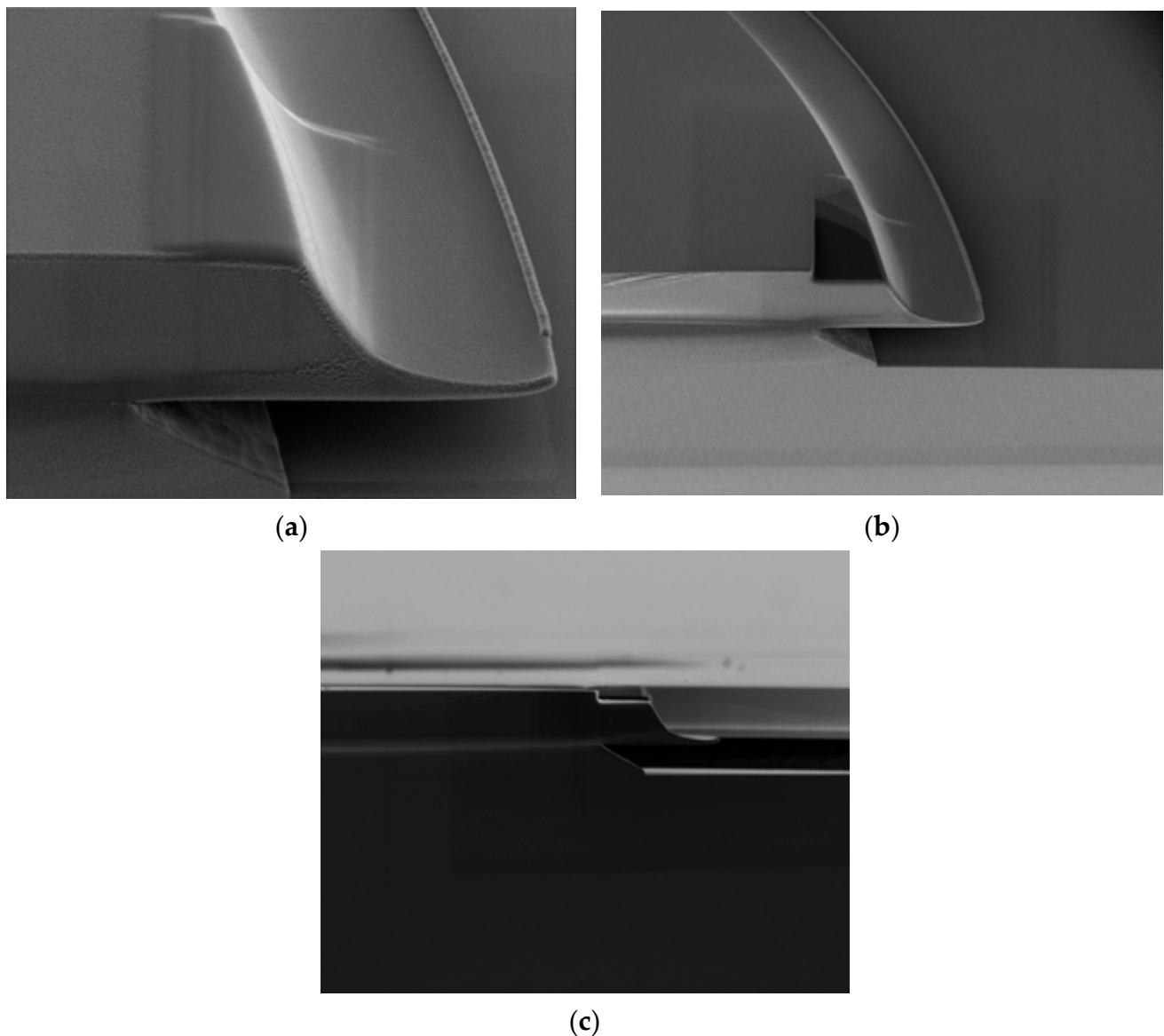
(**a**)

(**b**)

(**c**)

Figure 3. SEM images of the studied area: (**a**) chromium and platinum deposition performed; (**b**) the area removed by an ion beam; (**c**) side view of the studied area.

Three regions of the resonator diameter were selected for the study. In each area, 3 cuts were made using an ion beam, i.e., closer to the upper edge of the profile (Figure 4a), at the bend point of the profile (Figure 4b), and near the wedge (Figure 4c). A picture at a 250,000 magnification was taken in each region, showing the interface between the silicon structure and the metal. Then, the analysis of the obtained image was carried out by selecting the element border at the maximum gradient, followed by constructing the border profile (Figure 4). The length of the structure section in the image was 1.5 μm.
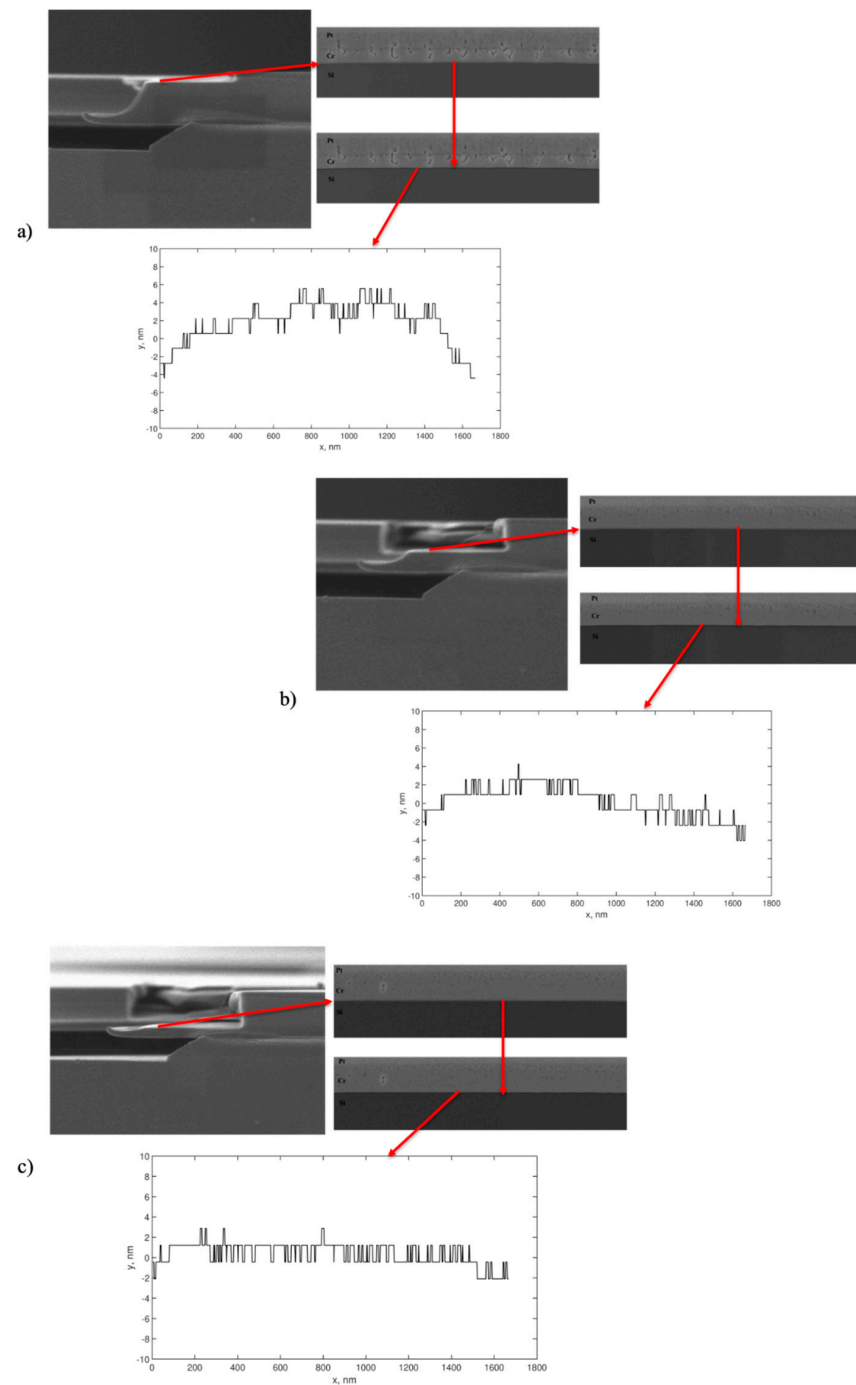

Figure 4. SEM images of profiles obtained using an ion beam, images of the Si-metal interface and the profile of the silicon element boundary (plotted along both axes; unit: nm) in different regions: (**a**) closer to the upper edge of the profile; (**b**) at the point of the profile bend; (**c**) near the wedge.

Since the profile of the studied area had a bend, we used the average value of the spread over the straight region, which was about 2 nm, to quantify the roughness.

3.2. Roughness Analysis Using Bruker AFM

At the same time, we used a Bruker atomic force microscope AFM to determine the roughness of the silicon disk resonator profile, as well as to test the method described in Section 3.1. The samples were scanned using a ScanAsyst Air probe with a V-shaped cantilever, with a nominal radius of the probe tip curvature of 2 nm.

Scanning was made in three areas (Figure 5), each of which was divided into several sub-areas.
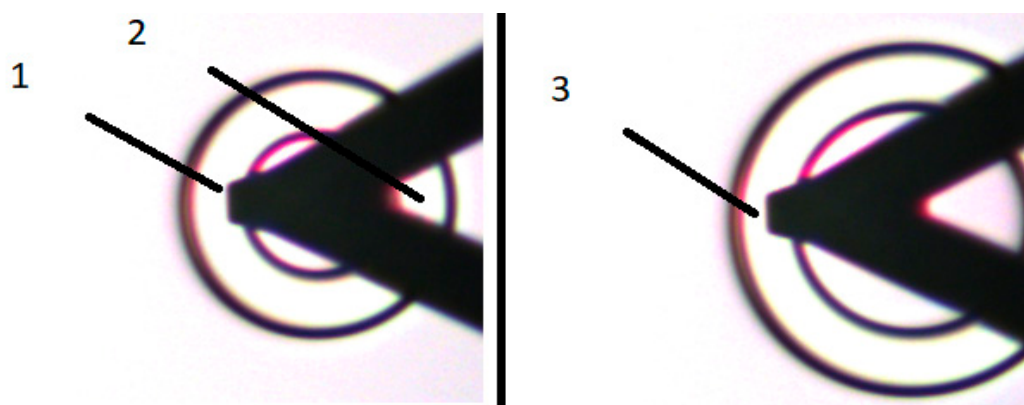

Figure 5. Scanned positions of the sample.

Figure 6 shows the AFM scan and its cross-section along the entire length of the ascent in area 1 in Figure 5.
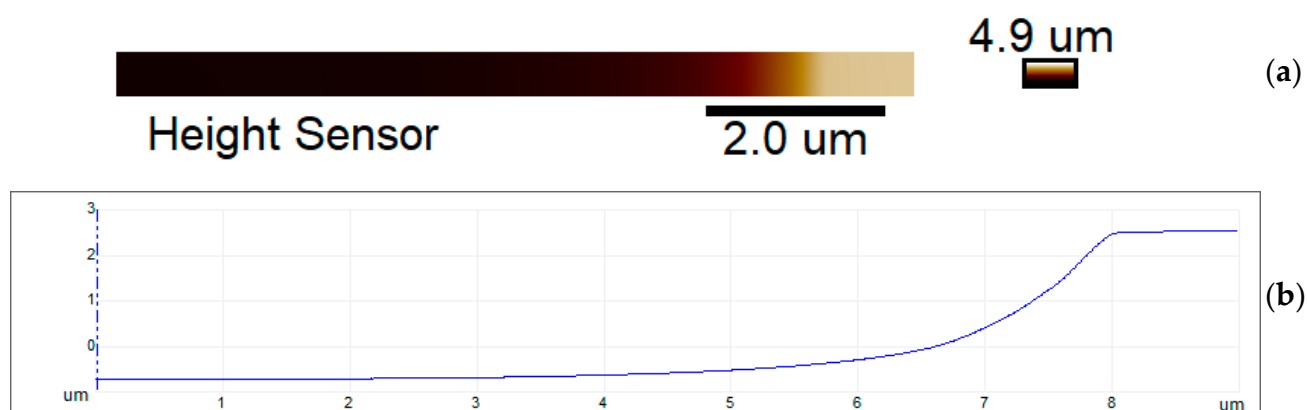

Figure 6. AFM scanning results of the surface profile of the silicon resonator: (**a**) scan of area 1 (resolution: 1024 pixels per line); (**b**) profile of area 1 plotted along the entire length of the ascent.

For a more accurate analysis of the roughness in area 1, three sub-areas with a length of 1 µm were determined (S1, at the beginning; S2, in the middle; S3, at the end of the rise). Thus, the lateral resolution was approximately 1 nm.

Figure 7 shows an AFM scan of sub-area S1 (its horizontal and vertical sections). The roughness of the sample was determined in terms of a vertical section (perpendicular to the scanning direction). The table (Figure 7a) shows the values of the horizontal and vertical distances between the markers indicated in Figure 7c. The colors of the markers correspond to the colors of the rows in the table. This approach maximizes the elimination of the influence of the sample geometry (tilt) on the difference in height between the peaks.
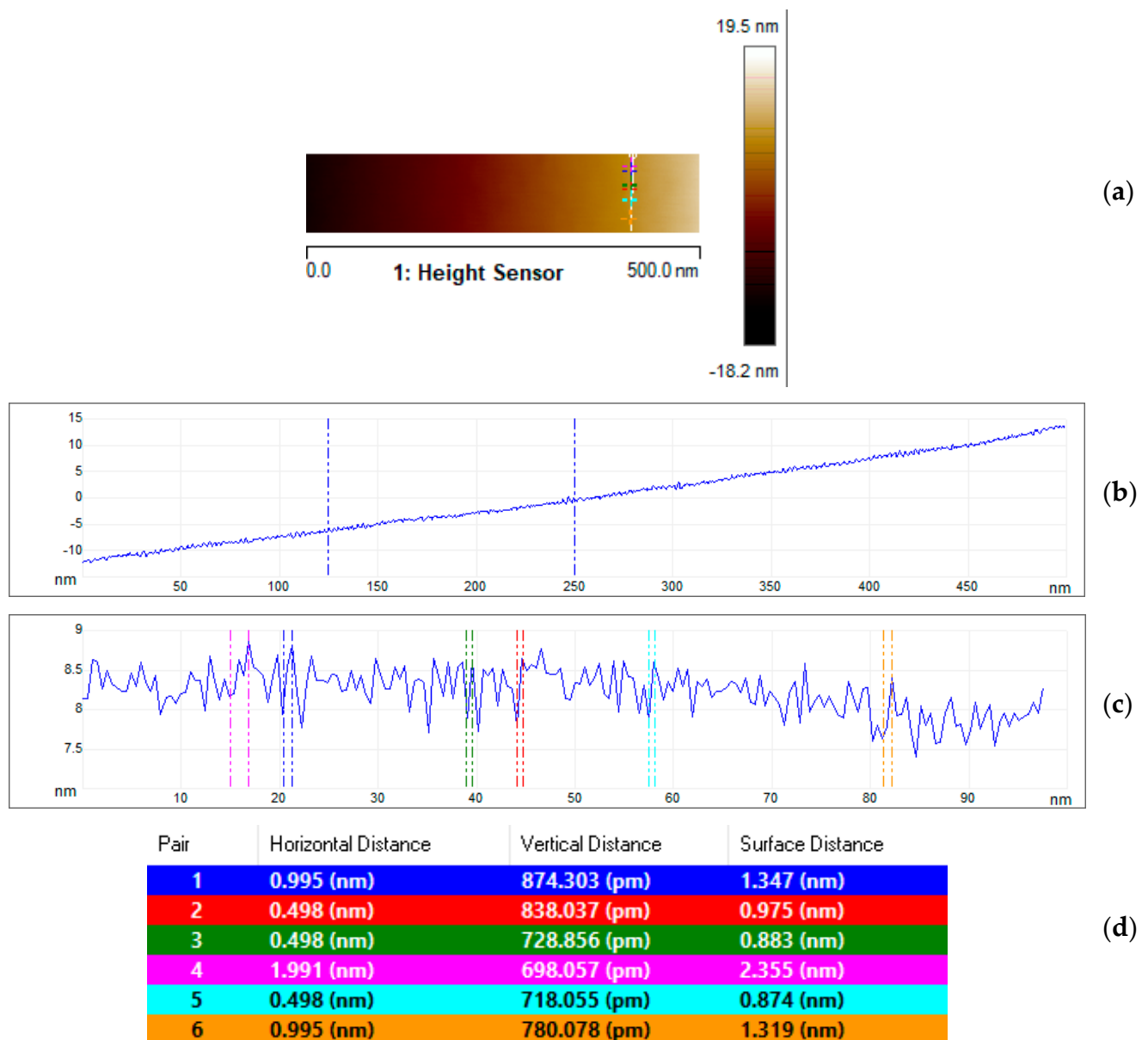
Figure 7. Result of the AFM scanning of sub-area S1: (**a**) scan of sub-area S1; (**b**) horizontal section of the scan of the Scheme 1; (**c**) cross-section of the scan of sub-area S1, the position of which is indicated by the white line in Figure 4a; (**d**) table of horizontal and vertical distances between markers indicated in Figure 4c.

The arithmetic mean of the profile deviation from the baseline R_a was 0.179 nm. The mean square deviation R_q was 0.225 nm.

Next, according to a similar principle, data were given for sub-areas S2 and S3 of area 1, similar sub-areas S4 and S5 of area 2, and S6 and S7 of area 3. The results are presented in Table 1.

Table 1. Results of the AFM scanning of the silicon resonator profile's surface.

Scanning Area	Scanning sub-Area	R_a (nm)	R_q (nm)
	S1	0.179	0.225
1	S2	0.246	0.313
	S3	0.906	1.130
2	S4	0.153	0.193
	S5	0.200	0.256
3	S6	0.194	0.243
	S7	0.279	0.340

The measured values of the arithmetic mean deviation of the R_a profile over the entire area did not exceed 1 nm, which is at the limit of the resolution of the technique. At the same time, it is obvious that as the steepness of the studied area increased, the roughness increased slightly. By comparing the surface roughness values of the silicon WGM resonator with two different methods, we can conclude that the results agree well with each other.

3.3. Results of the Surface Roughness of the WGM Resonator, Manufactured Using a Different Technological Approach

Previously, we presented a method for forming a silicon disk resonator with a wedge-shaped profile. The schematic of its cross-section is shown in Figure 8 [19].
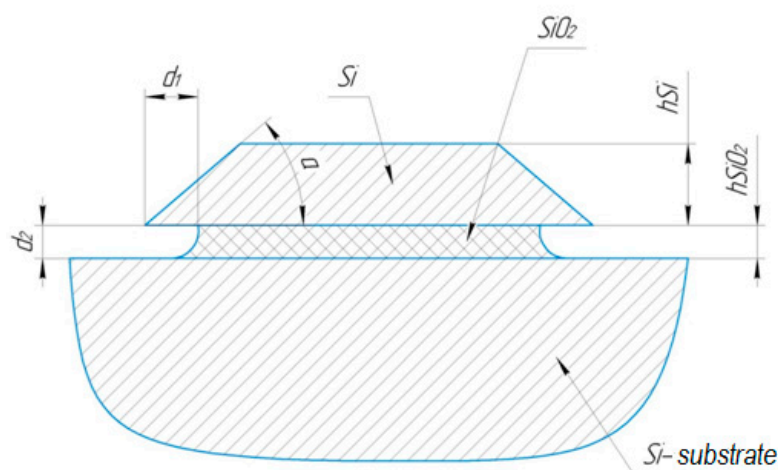

Figure 8. Schematic of the cross-section of the structure of the silicon WGM waveguide. Environment is air. h_{si}, the thickness (height) of the wedge-shaped waveguide; h_{SiO2}, thickness (height) of the dielectric layer; d_1, distance from the edge of the wedge to the beginning of the oxide beam (support); d_2, the gap between the edge of the wedge-shaped waveguide and the Si substrate; a, wedge angle [19].

The method of creating such a resonator was described earlier [19], and it involves the use of plasma-chemical etching to form the desired profile.

The roughness of such a silicon disk resonator was quantified using the method described in Section 3.1. It was about 30–40 nm.

4. Calculation of the Q-Factor and the Degree of Localization of the Light Flux in the Studied Silicon Disk Resonators

Based on the data obtained in Section 3, using the Q-factor calculation equation that takes into account the roughness of its surface [24,25], we made a preliminary approximate calculation of the Q-factors of the resonators:

$$Q_{ss\ B} \cong \frac{3\lambda^3 D}{16\pi^2 n\sigma^2 B^2},\tag{1}$$

where n is the refractive index of the host material, λ is the optical wavelength, and D is the diameter of the resonator, while σ and B are the RMS (root mean square) roughness and its correlation length, respectively.

To calculate Q-factors of real rough resonators, we used the finite-difference time-domain (FDTD) method. It assumes that a short pulse is launched into the studied object and the Q-factor is determined by its attenuation. A point dipole polarized in the tangential direction is a source to launch the field into the resonator. The fields of modes calculated in this way are shown in Figure 9. In Figure 9, it can be seen that the WGM field was localized near the edge of the disk. The square-shaped field strength closer to the center of the disk was the field from the exciting dipole. Due to the WGM resonance effect, the field of the exciting dipole attenuated stronger than the field of the resonant mode.

It should be noted that the FDTD method uses a short pulse containing a certain frequency spectrum to excite the field in a system. The shorter the pulse, the wider the spectrum, so it is not necessary to select the size of a resonator or the frequency of an input wave to fine-tune the resonance, while in the case of a wide pulse, several resonant frequencies can be excited in the resonator.

At the same time, we calculated the Q-factors of the resonators numerically using the FDTD method. Figure 9 shows the schematic of the field distribution in the disk resonator at the roughness value σ of 1 nm (Figure 9a) and at a roughness value σ of 40 nm (Figure 9b). The electric field was excited by four point dipole sources located near the edge of the disk along the straight lines $x = 0$ and $y = 0$. It can be seen in Figure 9a that the roughness σ of 1 nm did not negatively affect the formation of the WGM. The mode was formed near the edge of the disk (some distortions of the mode shape were associated with the presence of point sources), while the roughness σ of 40 nm led to a significant distortion of the excited mode (Figure 9b). In addition, as can be seen in Figure 9b, the field in the case of a large roughness was not completely localized inside the resonator. Therefore, there was a significant energy leakage, leading to a significant decrease in its Q-factor.

The Q-factor of the resonator was estimated from the decay time of a pulse launched into the resonator as following:

$$Q = \frac{2\pi f_R \log_{10} e}{2m},\qquad(2)$$

where f_R is the resonant frequency, e is the base of the natural logarithm, and m is the parameter of pulse attenuation. The time estimates for the modes in Figure 9 are shown in Table 2.

The results of the calculations are presented in Table 2.

Table 2. The results of the calculated Q-factors of silicon disk resonators with different surface roughness values.

	Test 1	Test 2
Surface roughness (nm)	1	40
Approximate calculation	10^7	1.8×10^4
Finite-difference time-domain (FDTD) calculation	10^7	1.3×10^4

The correlation length of the roughness was taken equal to 10σ [24].

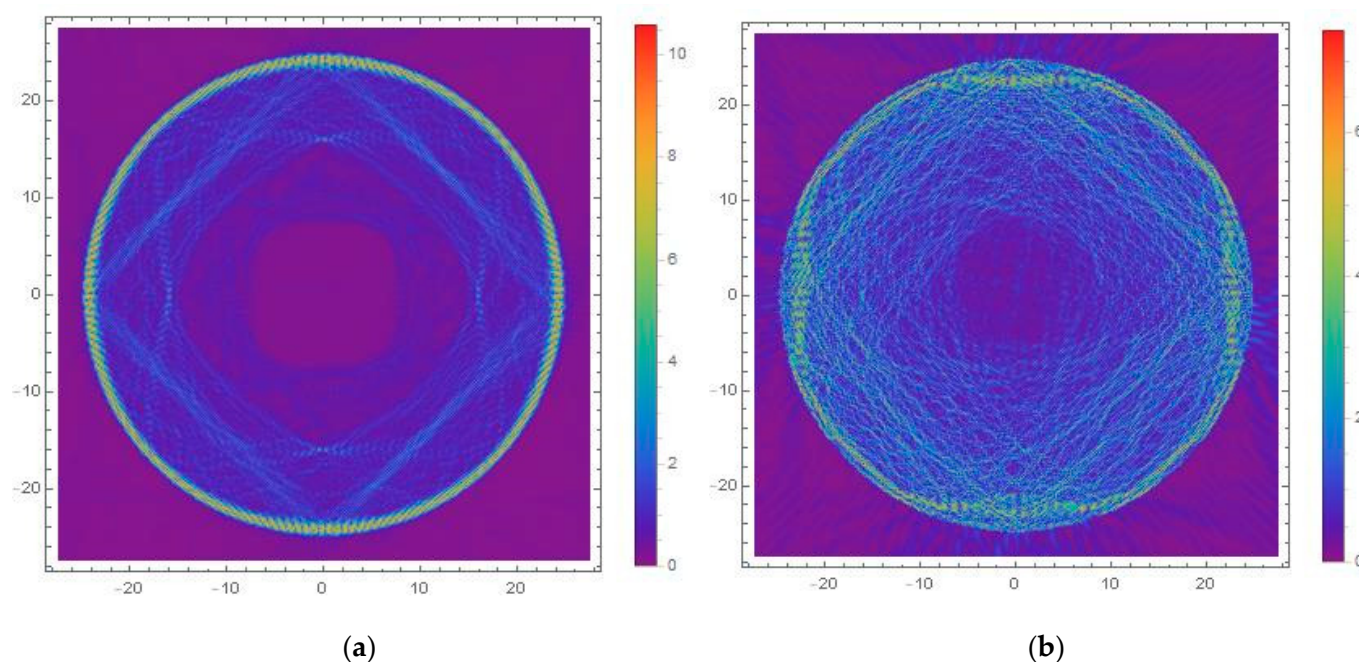(**a**)   (**b**)

Figure 9. Numerical simulation results of the electric field strengths in the resonator at different roughness values: (**a**) σ = 1 nm; (**b**) σ = 40 nm.

5. Conclusions

The methods for studying the surface roughness of a WGM resonator with a nonlinear profile presented in this work agree with each other. This makes it possible to obtain reliable information on the values of the surface roughness of structures with various non-standard profiles, as well as those of structures made of any materials compatible with silicon technology. Thus, we can say that this method can be used to analyze the influence of various technological approaches to the production of WGM resonators using silicon technology on the amount of surface roughness.

Based on the obtained data, it was found that in the case of a decrease in the surface roughness of the resonator by an order of magnitude (from 30–40 nm to 1–2 nm), its Q-factor increased by three orders of magnitude (from 10^4 to 10^7). It allows getting ultrahigh-Q silicon WGM resonators. Based on this fact, we can conclude that the surface roughness of the WGM resonator has a strong influence on its Q-factor. In addition, the technological approach to the production of resonators studied in this work is fully compatible with silicon technology, involves the use of group processing methods, which allows us to significantly expand the scope of their application, and increases prospects for integrating such resonators into PICs. In addition, the use of such resonators allows reducing the cost of each unit of a product, which will significantly increase prospects for their wide distribution and application in PICs.

Author Contributions: Conceptualization, A.V.Y. and V.V.S.; methodology, A.V.Y. and A.S.K.; software, A.S.K.; validation, V.V.A. and S.S.G.; formal analysis, A.V.Y. and A.S.K.; investigation, A.V.Y.; resources, V.V.A. and V.V.S.; data curation, V.V.A., V.V.S., and S.S.G.; writing—original draft preparation, A.V.Y.; writing—review and editing, D.V.G.; visualization, A.V.Y. and D.V.G.; supervision, V.V.A. and S.S.G.; project administration, V.V.A. and V.V.S.; funding acquisition, V.V.A. and S.S.G. All authors have read and agreed to the published version of the manuscript.

Conflicts of Interest: The authors declare no conflict of interest.

References

1. Gorodetsky, M.L. *Optical Microresonators with Giant Quality–Factor*; Fizmatlit: Moscow, Russia, 2011.
2. Monifi, F.; Friedlein, J.; Ozdemir, S.K.; Yang, L. A robust and tunable add–drop filter using whispering gallery mode microtoroid resonator. *J. Lightwave Technol.* **2012**, *30*, 3306–3315. [CrossRef]
3. Zhao, Y.; Wang, Q.; Meng, F.; Lin, Y.; Wang, S.; Li, Y.; Lin, B.; Cao, S.; Cao, J.; Fang, Z.; et al. High-finesse cavity external optical feedback DFB laser with hertz relative linewidth. *Opt. Lett.* **2012**, *37*, 4729–4731. [CrossRef]
4. Lewoczko-Adamczyk, W.; Pyrlik, C.; Hager, J.; Schwertfeger, S.; Wicht, A.; Peters, A.; Erbert, G.; Trankle, G. Ultra-narrow linewidth DFB-laser with optical feedback from a monolithic confocal Fabry-Perot cavity. *Opt. Express* **2015**, *23*, 9705–9709. [CrossRef]
5. Markvart, A.A.; Liokumovich, L.B.; Ushakov, N.A. Tunable optical delay lines based on a system of coupled whispering gallery mode resonators. *J. Phys. Conf. Ser.* **2019**, *1326*, 012017. [CrossRef]
6. Yoshiki, W.; Honda, Y.; Tetsumoto, T.; Furusawa, K.; Sekine, N.; Tanabe, T. All-optical tunable buffering with coupled Ultra-high Q whispering gallery mode microcavities. *Sci. Rep.* **2017**, *7*, 1–8. [CrossRef] [PubMed]
7. Wörhoff, K.; Heideman, R.G.; Leinse, A.; Hoekman, M. TriPleX: A versatile dielectric photonic platform. *Adv. Opt. Technol.* **2015**, *4*, 189–207. [CrossRef]
8. Iqbal, M.; Gleeson, M.A.; Spaugh, B.; Tybor, F.; Gunn, W.G.; Hochberg, M.; Baehr-Jones, T.; Bailey, R.C.; Gunn, L.C. Label-free biosensor arrays based on silicon ring resonators and high-speed optical scanning instrumentation. *IEEE J. Sel. Top. Quantum Electron.* **2010**, *16*, 654–661. [CrossRef]
9. Witzens, J.; Hochberg, M. Optical detection of target molecule induced aggregation of nanoparticles by means of high-Q resonators. *Opt. Express* **2011**, *19*, 7034–7061. [CrossRef]
10. Ramiro-Manzano, F.; Prtljaga, N.; Pavesi, L.; Pucker, G. Monolithic integration of High-Q wedge resonators with vertically coupled waveguides. In *Integrated Photonics: Materials, Devices, and Applications II, Proceedings of the SPIE 8767, International Society for Optics and Photonics, Grenoble, France, 24–27 April 2013*; SPIE: Bellingham, WA, USA, 2013; p. 876704.
11. Coillet, A.; Henriet, R.; Huy, K.P.; Jacquot, M.; Furfaro, L.; Balakireva, I.; Larger, L.; Chembo, Y.K. Microwave photonics systems based on whispering-gallery-mode resonators. *JoVE J. Vis. Exp.* **2013**, *78*, e50423. [CrossRef] [PubMed]
12. Herr, T.; Brasch, V.; Jost, J.D.; Wang, C.Y.; Kondratiev, N.M.; Grodestky, M.L.; Kippenberg, T.J. Temporal solitons in optical microresonators. *Nat. Photonics* **2014**, *8*, 146–152. [CrossRef]
13. Kippenberg, T.J.; Gaeta, A.L.; Lipson, M.; Gorodestky, M.L. Disiipative Kerr solitons in optical microresonators. *Science* **2018**, *361*, eaan8083. [CrossRef] [PubMed]
14. Suh, M.G.; Yang, Q.F.; Yang, K.Y.; Yi, X.; Vahala, K.J. Microresonator soliton dual-comb spectroscopy. *Science* **2016**, *354*, 600. [CrossRef]
15. Pavlov, N.G.; Lihachev, G.; Koptyaev, S.; Lucas, E.; Karpov, M.; Kondratiev, N.M.; Bilenko, I.A.; Kippenberg, T.J.; Gorodestky, M.L. Soliton dual frequency combs in crystalline microresonators. *Opt. Lett.* **2017**, *42*, 514. [CrossRef] [PubMed]
16. Liang, W.; Eliyahu, D.; Ilchenko, V.S.; Savchenkov, A.A.; Matsko, A.B.; Seidel, D.; Maleki, L. High spectral purity Kerr frequency comb radio frequency photonic oscillator. *Nat. Commun.* **2015**, *6*, 7957. [CrossRef] [PubMed]
17. Spencer, D.T.; Drake, T.; Briles, T.C.; Stone, J.; Sinclair, L.C.; Fredrick, C.; Li, Q.; Westly, D.; Ilic, B.R.; Bluestone, A.; et al. An optical-frequency synthesizer using integrated photonics. *Nat. Cell Biol.* **2018**, *557*, 81. [CrossRef] [PubMed]
18. Shitikov, A.E.; Kondratiev, N.M.; Lobanov, V.E.; Voloshin, A.S.; Bilenko, I.A. Fabrication and characterization of high-quality factor silicon WGM microresonators. In Proceedings of the European Conference on Lasers and Electro-Optics, Optical Society of America, Munich, Germany, 23–27 June 2019.
19. Yakuhina, A.; Kadochkin, A.; Amelichev, V.; Gorelov, D.; Generalov, S. Research of constructive and technological methods for forming a silicon disk resonator with whispering gallery modes. *Photonics* **2020**, *7*, 31. [CrossRef]
20. Chen, T.; Lee, H.; Vahala, K.J. Design and characterization of whispering-gallery spiral waveguides. *Opt. Express* **2014**, *22*, 5196–5208. [CrossRef]
21. Yakuhina, A.; Kadochkin, A.; Svetukhin, V.; Gorelov, D.; Generalov, S.; Amelichev, V. Investigation of side wall roughness effect on optical losses in a multimode Si3N4 waveguide formed on a quartz substrate. *Photonics* **2020**, *7*, 104. [CrossRef]

22. Kizu, R.; Misumi, I.; Hirai, A.; Gonda, S. Line edge roughness measurement on vertical sidewall for reference metrology using a metrological tilting atomic force microscope. *J. Micro/Nanolithography MEMS MOEMS* **2020**, *19*, 014003. [CrossRef]

23. Takamasu, K.; Takahashi, S.; Kawada, H.; Ikota, M. Linewidth roughness of advanced semiconductor features using focused ion beam and planar-transmission electron microscope as reference metrology. *J. Micro/Nanolithography MEMS MOEMS* **2018**, *17*, 041010. [CrossRef]

24. Lin, G.; Henriet, R.; Coillet, A.; Jacquot, M.; Furfaro, L.; Cibiel, G.; Larger, L.; Chembo, Y.K. Dependence of quality factor on surface roughness in crystalline whispering-gallery mode resonators. *Opt. Lett.* **2018**, *43*, 495–498. [CrossRef] [PubMed]

25. Gorodetsky, M.L.; Pryamikov, A.D.; Ilchenko, V.S. Rayleigh scattering in high-Q microspheres. *J. Opt. Soc. Am. B* **2000**, *17*, 1051. [CrossRef]